

Neural Transformation Learning for Deep Anomaly Detection Beyond Images

Chen Qiu^{1,2} Timo Pfrommer¹ Marius Kloft² Stephan Mandt³ Maja Rudolph¹

Abstract

Data transformations (e.g. rotations, reflections, and cropping) play an important role in self-supervised learning. Typically, images are transformed into different views, and neural networks trained on tasks involving these views produce useful feature representations for downstream tasks, including anomaly detection. However, for anomaly detection beyond image data, it is often unclear which transformations to use. Here we present a simple end-to-end procedure for anomaly detection with *learnable* transformations. The key idea is to embed the transformed data into a semantic space such that the transformed data still resemble their untransformed form, while different transformations are easily distinguishable. Extensive experiments on time series demonstrate that we significantly outperform existing methods on the one-vs.-rest setting but also on the more challenging n -vs.-rest anomaly-detection task. On tabular datasets from the medical and cybersecurity domains, our method learns domain-specific transformations and detects anomalies more accurately than previous work.

1. Introduction

Many recent advances in anomaly detection rely on the paradigm of data augmentation. In the self-supervised setting, especially for image data, predefined transformations such as rotations, reflections, and cropping are used to generate varying *views* of the data. This idea has led to strong anomaly detectors based on either transformation prediction (Golan & El-Yaniv, 2018; Wang et al., 2019b; Hendrycks et al., 2019) or using representations learned using these views (Chen et al., 2020) for downstream anomaly detection tasks (Sohn et al., 2020; Tack et al., 2020).

Unfortunately, for data other than images, such as time series or tabular data, it is much less well known which transformations are useful, and it is hard to design these trans-

formations manually. This paper studies self-supervised anomaly detection for data types beyond images. We develop **neural transformation learning for anomaly detection (NeuTraL AD)**: a simple end-to-end procedure for anomaly detection with *learnable* transformations. Instead of manually designing data transformations to construct auxiliary prediction tasks that can be used for anomaly detection, we derive a single objective function for jointly learning useful data transformations and anomaly thresholding. As detailed below, the idea is to learn a variety of transformations such that the transformed samples share semantic information with their untransformed form, while different views are easily distinguishable.

NeuTral AD has only two components: a fixed set of learnable transformations and an encoder model. Both elements are jointly trained on a noise-free, **deterministic contrastive loss (DCL)** designed to learn faithful transformations. Our DCL is different from other contrastive losses in representation learning (Gutmann & Hyvärinen, 2010; 2012; Mnih & Kavukcuoglu, 2013; Oord et al., 2018; Chen et al., 2020) and image anomaly detection (Tack et al., 2020; Sohn et al., 2020), all of which use negative samples from a noise distribution. In contrast, our approach leads to a non-stochastic objective that neither needs any additional regularization or adversarial training (Tamkin et al., 2020) and can be directly used as the anomaly score.

Our approach leads to a new state of the art in anomaly detection beyond images. For time series and tabular data, NeuTral AD significantly improves the anomaly detection accuracy. For example, in an epilepsy time series dataset, we raised the state-of-the-art from an AUC of 82.6% to 92.6% (+10%). On an Arrhythmia tabular dataset, we raised the F1 score by +2.9 percentage points to an accuracy of 60.3.

Our paper is structured as follows. We first discuss related work (Section 2) and present NeuTral AD in Section 3. In Section 3.2 we discuss its advantages for neural transformation learning in comparison to other self-supervised learning objectives. Experimental results are presented in Section 4.

2. Related Work

Deep Anomaly Detection. Recently, there has been a rapidly growing interest in developing deep-learning

¹Bosch Center for AI ²TU Kaiserslautern ³UC Irvine. Correspondence to: Maja Rudolph <maja.rudolph@de.bosch.com>.

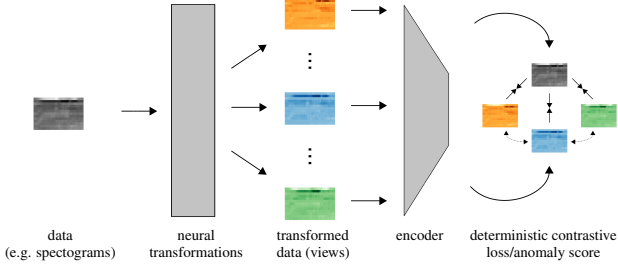


Figure 1. NeuTraL AD is an end-to-end procedure for self-supervised anomaly detection with *learnable* neural transformations. Each sample is transformed by a set of learned transformations and then embedded into a semantic space. The transformations and the encoder are trained jointly on a contrastive objective (Equation (2)), which is also used to score anomalies.

approaches for anomaly detection (Ruff et al., 2020). While deep learning—by removing the burden of manual feature engineering for complex problems—has brought about tremendous technological advances, its application to anomaly detection is rather recent. Related work on deep anomaly detection includes deep autoencoder variants (Principi et al., 2017; Zhou & Paffenroth, 2017; Chen & Konukoglu, 2018), deep one-class classification (Erfani et al., 2016; Ruff et al., 2019b;a), deep generative models (Schlegl et al., 2017; Deecke et al., 2018), and outlier exposure (Hendrycks et al., 2018; Goyal et al., 2020).

Self-supervised anomaly detection has led to drastic improvements in detection accuracy (Golan & El-Yaniv, 2018; Hendrycks et al., 2019; Wang et al., 2019b; Sohn et al., 2020; Tack et al., 2020). For instance, Golan & El-Yaniv (2018) and Wang et al. (2019b) augment the data and learn to predict which transformation was applied. After training, the resulting classifier is used for anomaly detection.

An alternative approach to self-supervised anomaly detection is to train a classifier on a contrastive loss to tell if two views are of the same original image. This leads to strong representations (Chen et al., 2020), which can be used for anomaly detection (Sohn et al., 2020; Tack et al., 2020).

Bergman & Hoshen (2020) study how to extend self-supervised anomaly detection to other domains beyond images. Similar to Golan & El-Yaniv (2018) and Wang et al. (2019b), their approach is based on transformation prediction, but they consider the open-set setting. For tabular data, they use random affine transformations. We study the same datasets, but our method *learns* the transformations and achieves consistently higher performance (see Section 4).

Self-Supervised Learning. Self-supervised learning typically relies on data augmentation for auxiliary tasks (Doersch et al., 2015; Noroozi & Favaro, 2016; Misra et al., 2016; Zhang et al., 2017; Gidaris et al., 2018). The net-

works trained on these auxiliary tasks (e.g. patch prediction (Doersch et al., 2015), solving jigsaw-puzzles (Noroozi & Favaro, 2016), cross-channel prediction (Zhang et al., 2017), or rotation prediction (Gidaris et al., 2018)) are used as feature extractors for downstream tasks. While many of these methods are developed for images, Misra et al. (2016) propose temporal order verification as an auxiliary task for self-supervised learning of time-series representations.

Contrastive Representation Learning. Many recent self-supervised methods have relied on the InfoMax principle (Linsker, 1988; Hjelm et al., 2018). These methods are trained on the task to maximize the **mutual information (MI)** between the data and their context (Oord et al., 2018) or between different “views” of the data (Bachman et al., 2019). Computing the mutual information in these settings is often intractable and various approximation schemes and bounds have been introduced (Tschannen et al., 2019). By using noise contrastive estimation (Gutmann & Hyvärinen, 2010; 2012) to bound MI, Oord et al. (2018) bridge the gap between contrastive losses for MI-based representation learning and the use of contrastive losses in discriminative methods for representation learning (Hadsell et al., 2006; Mnih & Kavukcuoglu, 2013; Dosovitskiy et al., 2015; Bachman et al., 2019; Chen et al., 2020). We also use a contrastive loss. But while the contrastive loss of Chen et al. (2020) (which is used for anomaly detection of images in Sohn et al. (2020); Tack et al. (2020),) contrast two views of the same sample with views of other samples in the mini-batch, NeuTraL AD is tasked with determining the original version of a sample from different views of the same sample. The dependence on only a single sample is advantageous for scoring anomalies at test time and enables us to learn the data transformations (discussed further in Section 3.2).

Learning Data Augmentation Schemes. The idea of learning data augmentation schemes is not new. “AutoAugmentation” has usually relied on composing hand crafted data augmentations (Ratner et al., 2017; Cubuk et al., 2018; Zhang et al., 2019; Ho et al., 2019; Lim et al., 2019). Tran et al. (2017) learn Bayesian augmentation schemes for neural networks, and Wong & Kolter (2020) learn perturbation sets for adversarial robustness. Though their setting and approach are different, our work is most closely related to Tamkin et al. (2020), who study how to generate views for representation learning in the framework of Chen et al. (2020). They parametrize their “viewmakers” as residual perturbations, which are trained adversarially to avoid trivial solutions where the views share no semantic information with the original sample (discussed in Section 3.2).

NeuTraL AD falls into the area of deep, self-supervised anomaly detection, with the the core novelty of learning the transformations so that we can effectively use them for anomaly detection beyond images. Our method receives

whole time series or tabular data as input. For time series, this is a remarkable difference to prevalent work on anomaly detection *within* time series (e.g. Shen et al., 2020), which output anomaly scores per time point, but not for the sequence as a whole. Additional approaches to time-series anomaly detection include shallow (Hyndman et al., 2015; Baragona & Battaglia, 2007) and deep-learning approaches based on modeling (Munir et al., 2018), on autoencoders (Kieu et al., 2018), or one-class classification (Shen et al., 2020).

3. Neural Transformation Learning for Deep Anomaly Detection

We develop **neural transformation learning for anomaly detection (NeuTraL AD)**, a deep anomaly detection method based on contrastive learning for general data types. We first describe the approach in Section 3.1. In Section 3.2, we provide theoretical arguments why alternative contrastive loss functions are less suited for anomaly detection.

3.1. Proposed Method: NeuTraL AD

Our method, **NeuTraL AD**, is a simple pipeline with two components: a set of learnable transformations, and an encoder. Both are trained jointly on a **deterministic contrastive loss (DCL)**. The objective has two purposes. During training, it is optimized to find the parameters of the encoder and the transformations. During testing, the **DCL** is also used to score each sample as either an inlier or an anomaly.

Learnable Data Transformations. We consider a data space \mathcal{X} with samples $\mathcal{D} = \{x^{(i)} \sim \mathcal{X}\}_{i=1}^N$. We also consider K transformations $\mathcal{T} := \{T_1, \dots, T_K | T_k : \mathcal{X} \rightarrow \mathcal{X}\}$. We assume here that the transformations are learnable, i.e., they can be modeled by any parameterized function whose parameters are accessible to gradient-based optimization and we denote the parameters of transformation T_k by θ_k . In our experiments we use feed-forward neural networks for T_k . Note that in Section 3.2, we use the same notation also for fixed transformations (such as rotations and cropping).

Deterministic Contrastive Loss (DCL). A key ingredient of **NeuTraL AD** is a new objective. The **DCL** encourages each transformed sample $x_k = T_k(x)$ to be similar to its original sample x , while encouraging it to be dissimilar from other transformed versions of the same sample, $x_l = T_l(x)$ with $l \neq k$. We define the score function of two (transformed) samples as

$$h(x_k, x_l) = \exp(\text{sim}(f_\phi(T_k(x)), f_\phi(T_l(x))) / \tau), \quad (1)$$

where τ denotes a temperature parameter, and the similarity is defined as the cosine similarity $\text{sim}(z, z') := z^T z' / \|z\| \|z'\|$ in an embedding space \mathcal{Z} . The encoder

$f_\phi(\cdot) : \mathcal{X} \rightarrow \mathcal{Z}$ serves as a features extractor. The **DCL** is

$$\mathcal{L} := \mathbb{E}_{x \sim \mathcal{D}} \left[- \sum_{k=1}^K \log \frac{h(x_k, x)}{h(x_k, x) + \sum_{l \neq k} h(x_k, x_l)} \right]. \quad (2)$$

The parameters of **NeuTraL AD** $\theta = [\phi, \theta_{1:K}]$ consist of the parameters ϕ of the encoder, and the parameters $\theta_{1:K}$ of the learnable transformations. All parameters θ are optimized jointly by minimizing Equation (2).

A schematic of **NeuTraL AD** is in Figure 1. Each sample is transformed by a set of learnable transformations and then embedded into a semantic space. The transformations and the encoder are trained jointly on the **DCL** (Equation (2)), which is also used to score anomalies. The numerator of the **DCL** encourages the transformed samples to align with the original sample (in the embedding space of the encoder), while the denominator pushes the embeddings of different views of a sample apart from each other.

Anomaly Score. One advantage of our approach over other methods is that our training loss is also our anomaly score. Based on Equation (2), we define an anomaly score $S(x)$ as

$$S(x) = \sum_{k=1}^K \log \frac{h(x_k, x)}{h(x_k, x) + \sum_{l \neq k} h(x_k, x_l)}. \quad (3)$$

Since the score is deterministic, it can be straightforwardly evaluated for new data points x without negative samples.

This concludes the proposed loss function. We stress that it is extremely simple and does not need any additional regularization. However, it is not trivial to see why other proposed self-supervised approaches are less well suited for anomaly detection without imposing constraints on the types of transformations. To this end, we establish theoretical requirements and desiderata for neural transformation learning.

3.2. A Theory of Neural Transformation Learning

To learn transformations for self-supervised anomaly detection we pose two requirements.

Requirement 1 (Semantics). *The transformations should produce views that share relevant semantic information with the original data.*

Requirement 2 (Diversity). *The transformations should produce diverse views of each sample.*

A valid loss function for neural transformation learning should avoid solutions that violate either of these requirements. There are plenty of transformations that would violate Requirement 1 or Requirement 2. For example, a constant transformation $T_k(x) = c_k$, where c_k is a constant that does not depend on x , would violate the semantic requirement, whereas the identity $T_1(x) = \dots = T_K(x) = x$ violates the diversity requirement.

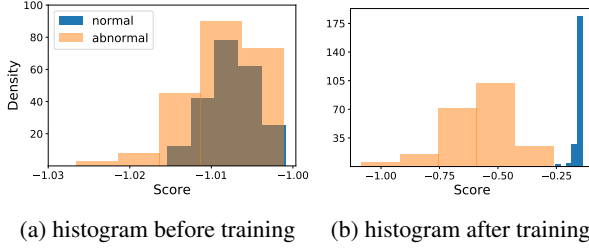


Figure 2. While the histogram of anomaly scores (computed using Equation (3)) is similar for inliers (blue) and anomalies (orange) before training, this changes drastically after training, and held-out inliers and anomalies become easily distinguishable. The data come from the **SAD** experiments described in Section 4

We argue thus that for self-supervised anomaly detection, the learned transformations need to negotiate the trade-off between semantics and diversity with the two examples as edge-cases on a spectrum of possibilities. Without semantics, i.e. without dependence on the input data, an anomaly detection method can not decide whether a new sample is normal or an anomaly. And without variability in learning transformations, the self-supervised learning goal is not met.

We now put the benefits of **NeuTraL AD** into perspective by comparing the approach with two other approaches that use data transformations for anomaly detection:

1. The first approach is the transformation prediction approach by Wang et al. (2019b). Here, $f_\phi(\cdot) : \mathcal{X} \rightarrow \mathbb{R}^K$ is a deep classifier¹ that outputs K values $f_\phi(x)_1 \cdots f_\phi(x)_K$ proportional to the log-probabilities of the transformations. The transformation prediction loss is a softmax classification loss,

$$\mathcal{L}_P := \mathbb{E}_{x \sim \mathcal{D}} \left[- \sum_{k=1}^K \log \frac{\exp f_\phi(x)_k}{\sum_{l=1:K} \exp f_\phi(x)_l} \right]. \quad (4)$$

2. We also consider (Chen et al., 2020), who define a contrastive loss on each minibatch of data $\mathcal{M} \subset \mathcal{D}$ of size $N = |\mathcal{M}|$. For each gradient step, they sample a minibatch and two transformations $T_1, T_2 \sim \mathcal{T}$ from the family of transformations, which are applied to all the samples to produce $x_k^{(i)} = T_k(x^{(i)})$. The loss function is given by $\mathcal{L}_C(\mathcal{M}) := \sum_{i=1}^N \mathcal{L}_C(x_1^{(i)}, x_2^{(i)}) + \mathcal{L}_C(x_2^{(i)}, x_1^{(i)})$, where

$$\begin{aligned} \mathcal{L}_C(x_1^{(i)}, x_2^{(i)}) &:= -\log h(x_1^{(i)}, x_2^{(i)}) \\ &+ \log \left[\sum_{j=1}^N h(x_1^{(i)}, x_2^{(j)}) + \sum_{j=1}^N \mathbb{1}_{[j \neq i]} h(x_1^{(i)}, x_1^{(j)}) \right]. \end{aligned} \quad (5)$$

¹even though here f_ϕ is a classifier, we refer to it as the encoder in the discussion below.

With hand-crafted, fixed transformations, these losses produce excellent anomaly detectors for images (Golan & El-Yaniv, 2018; Wang et al., 2019b; Sohn et al., 2020; Tack et al., 2020). Since it is not always easy to design transformations for new application domains, we study their suitability for *learning* data transformations.

We argue that \mathcal{L}_P and \mathcal{L}_C are less well suited for transformation learning than \mathcal{L} :

Proposition 1. *The ‘constant’ edge-case $f_\phi(T_k(x)) = C c_k$, where c_k is a one-hot vector encoding the k^{th} position (i.e. $c_{kk} = 1$) tends towards the minimum of \mathcal{L}_P (Equation (4)) as the constant C goes to infinity.*

Proposition 2. *The ‘identity’ edge-case $T_k(x) = x$ with adequate encoder f_ϕ is a minimizer of \mathcal{L}_C (Equation (5)).*

The proof of these propositions is in Appendix A. The intuition is simple. Transformations that only encode which transformation was used make transformation prediction easy (Proposition 1), whereas the identity makes any two views of a sample identical, which can then be easily recognized as a positive pair by \mathcal{L}_C (Proposition 2).

The propositions highlight a serious issue with using \mathcal{L}_P or \mathcal{L}_C for transformation learning and anomaly detection. Should the optimization reach the edge-cases of Propositions 1 and 2, \mathcal{L}_P and \mathcal{L}_C incur the same loss irrespective of whether the inputs are normal or abnormal data. Here are three remedies that can help avoid the trivial edge-cases: Through careful *parametrization* one can define $T_k(\cdot; \theta_k)$ in a way that explicitly excludes the edge cases. Beware that the transformation family might contain other members that violate Requirement 1 or Requirement 2. The second potential remedy is *regularization* that explicitly encourages Requirements 1 and 2, e.g. based on the InfoMax principle (Linsker, 1988) or norm constraints. Finally, one can resort to *adversarial training*.

Tamkin et al. (2020) use all three of these remedies to learn “viewmakers” using the contrastive loss \mathcal{L}_C ; They parametrize the transformations as residual perturbations, which are regularized to the ℓ_p ball and trained adversarially. In contrast, under **NeuTraL AD** there are no restrictions on the architecture of the transformations, as long as Equation (2) can be optimized (i.e. the gradient is well defined). The **DCL** is an adequate objective for training the encoder and transformations jointly as it manages the trade-off between Requirements 1 and 2.

Proposition 3. *The edge-cases of Propositions 1 and 2 do not minimize \mathcal{L} (**DCL**, Equation (2)).*

The proof is in Appendix A. The numerator of Equation (2) encourages transformed samples to resemble their original version (i.e. the semantic requirement) and the denominator encourages the diversity of transformations. The result

of our well-balanced objective is a heterogeneous set of transformations that model various relevant aspects of the data. The transformations and the encoder need to highlight salient features of the data such that a low loss can be achieved. After training, samples from the data class have a low anomaly score while anomalies are handled less well by the model and as a result have a high score.

Figure 2 shows empirical evidence for this. We observe that, while the histogram of anomaly scores (computed using Equation (3)) is similar for inliers and anomalies before training, this changes drastically after training, and held-out inliers and anomalies become easily distinguishable.

There’s another advantage of using the **DCL** for self-supervised anomaly detection. Unlike most other contrastive losses, the “negative samples” are not drawn from a noise distribution (e.g. other samples in the minibatch) but constructed deterministically from x . Dependence on the minibatch for negative samples would need to be accounted for at test time. In contrast, the deterministic nature of Equation (3) makes it a simple choice for anomaly detection.

4. Empirical Study: Deep Anomaly Detection of Time Series and Tabular Data

We developed **NeuTraL AD** for deep anomaly detection beyond images, so we consider various application domains involving multiple data types. For image data, strong self-supervised baselines exist that benefit from hand-crafted transformations. We do not expect any benefit from using **NeuTraL AD** there. Our focus here is on time series and tabular data, which are important in many application domains of anomaly detection. Our study finds that **NeuTraL AD** improves detection accuracy over the state of the art.

4.1. Evaluation Protocol

We compare **NeuTraL AD** to prevalent shallow and deep anomaly-detection baselines using two evaluation protocols: the standard ‘one-vs.-rest’ and the more challenging ‘ n -vs.-rest’ evaluation protocol. Both settings turn a classification dataset into a quantifiable anomaly-detection benchmark.

one-vs-rest. This evaluation setup has been used in virtually all papers on deep anomaly detection published at top-tier venues (e.g. Ruff et al., 2019a; Hendrycks et al., 2019; Ruff et al., 2018; Golan & El-Yaniv, 2018; Deecke et al., 2018; Akcay et al., 2018; Abati et al., 2019; Perera et al., 2019; Wang et al., 2019a; Bergman & Hoshen, 2020; Kim et al., 2019). For ‘one-vs.-rest’, the dataset is split by the N class labels, creating N one class classification tasks; the models are trained on data from one class and tested on a test set with examples from all classes. The samples from other classes should be detected as anomalies.

n-vs-rest. We also evaluate on the more challenging n -vs.-rest protocol, where n classes (for $1 < n < N$) are treated as normal and the remaining classes provide the anomalies in the test and validation set. By increasing the variability of what is considered normal data, one-class classification becomes more challenging.

4.2. Shallow and Deep Anomaly Detection Baselines

We study **NeuTraL AD** in comparison to a number of unsupervised and self-supervised anomaly detection methods.

Traditional Anomaly Detection Baselines. We chose three popular anomaly detection baselines: The **one-class SVM (OC-SVM)**, a kernel-based method, **isolation forest (IF)**, a tree-based model which aims to isolate anomalies (Liu et al., 2008), and **local outlier factor (LOF)**, which uses density estimation with k -nearest neighbors.

Deep Anomaly Detection Baselines. Next, we include three deep anomaly detection methods, **Deep SVDD** (Ruff et al., 2018), which fits a one-class SVM in the feature space of a neural net, **DROCC** (Goyal et al., 2020), which fits a one-class classifier with artificial outlier exposure, and **DAGMM** (Zong et al., 2018), which estimates the density in the latent space of an autoencoder.

Self-Supervised Anomaly Detection Baselines. We also choose two self-supervised baselines, which are technically also deep anomaly detection methods. **GOAD** (Bergman & Hoshen, 2020) is a distance-based classification method based on random affine transformations. (Wang et al., 2019b) is a softmax-based classification method based on hand-crafted transformations, which show impressive performance on images. We adopt their pipeline to time series here by crafting specific time-series transformations (described in appendix B).

Anomaly Detection Baselines for Time Series. Finally, we also include two baselines that are specifically designed for time series data: The **RNN-based model (RNN)** directly models the data distribution $p(x_{1:T}) = \prod p(x_t|x_{<t})$ and uses the log-likelihood as the anomaly score. Details on the architecture are in Appendix B. **LSTM-ED** (Malhotra et al., 2016) is an encoder-decoder time-series model where anomaly score is based on the reconstruction error.

4.3. Anomaly Detection of Time Series

Our goal is to detect abnormal time series on a *whole-sequence level*. This is a different set-up than novelty detection within time series, but also very important in practice.

For example, one might want to detect abnormal sounds, or find production quality issues by detecting abnormal sensor measurements recorded over the duration of producing a batch. Other applications are sports and health monitoring;

Table 1. Average AUC with standard deviation for one-vs-rest anomaly detection on time series datasets.

	OC-SVM	IF	LOF	RNN	LSTM-ED	Deep SVDD	DAGMM	GOAD	DROCC	fixed Ts	NeuTraL AD
SAD	95.3	88.2	98.3	81.5 \pm 0.4	93.1 \pm 0.5	86.0 \pm 0.1	80.9 \pm 1.2	94.7 \pm 0.1	85.8 \pm 0.8	96.7 \pm 0.1	98.9 \pm 0.1
NATOPS	86.0	85.4	89.2	89.5 \pm 0.4	91.5 \pm 0.3	88.6 \pm 0.8	78.9 \pm 3.2	87.1 \pm 1.1	87.2 \pm 1.4	78.4 \pm 0.4	94.5 \pm 0.8
CT	97.4	94.3	97.8	96.3 \pm 0.2	79.0 \pm 1.1	95.7 \pm 0.5	89.8 \pm 0.7	97.7 \pm 0.1	95.3 \pm 0.3	97.9 \pm 0.1	99.3 \pm 0.1
EPSY	61.1	67.7	56.1	80.4 \pm 1.8	82.6 \pm 1.7	57.6 \pm 0.7	72.2 \pm 1.6	76.7 \pm 0.4	85.8 \pm 2.1	80.4 \pm 2.2	92.6 \pm 1.7
RS	70.0	69.3	57.4	84.7 \pm 0.7	65.4 \pm 2.1	77.4 \pm 0.7	51.0 \pm 4.2	79.9 \pm 0.6	80.0 \pm 1.0	87.7 \pm 0.8	86.5 \pm 0.6

an abnormal movement pattern during sports can be indicative of fatigue or injury; whereas anomalies in health data can point to more serious issues.

We study **NeuTraL AD** on a selection of datasets that are representative of these varying domains. The datasets come from the UEA multivariate time series classification archive² (Bagnall et al., 2018).

Time Series Datasets

- **SAD**: Sound of ten Arabic digits, spoken by 88 speakers. The dataset has 8800 samples, which are stored as 13 Mel Frequency Cepstral Coefficients (MFCCs). The data is zero padded to have the same time length of 50.
- **Naval air training and operating procedures standardization (NATOPS)**: The data is originally from a motion detection competition of various movement patterns used to control planes in naval air training. The data has six classes of distinct actions. Each sample is a sequence of x, y, z coordinates for eight body parts of length 51.
- **Character trajectories (CT)**: The data consists of 2858 character samples from 20 classes, captured using a WACOM tablet. Each instance is a 3-dimensional pen tip velocity trajectory. The data is truncated to the length of the shortest, which is 182.
- **Epilepsy (EPSY)**: The data was generated with healthy participants simulating four different activities: walking, running, sawing with a saw, and seizure mimicking whilst seated. The data has totally 275 cases, each is a 3-dimensional sequence with a length of 203.
- **Racket sports (RS)**: The data is a record of university students playing badminton or squash whilst wearing a smart watch, which measures the x, y, z coordinates for both the gyroscope and accelerometer. Sport and stroke type separate the data into four classes. Each sample is a 6-d sequence with a length of 30.

We compare **NeuTraL AD** to all baselines from Section 4.2 on these datasets under the one-vs-rest setting. Additionally, we study how the methods adapt to increased variability of inliers by exploring **SAD** and **NATOPS** under the n -vs-rest

²from which we selected datasets on which supervised multi-class classification methods achieve strong results (Ruiz et al., 2020). Only datasets with separable classes can be repurposed for one-class classification

setting for varying number of classes n considered normal.

Implementation Details We parameterize the learnable transformations of **NeuTraL AD** multiplicatively $T_k(x) = M_k(x) \odot x$ (elementwise multiplication). The masks M_k are each a stack of three residual blocks with instance normalization layers plus one convolutional layer with sigmoid activation function. All bias terms are zero. For a fair comparison, we use the same number of 12 transformations in **NeuTraL AD**, **GOAD**, and the classification based method (fixed T) for which we manually designed appropriate transformations. In section 4.5 we make a more detailed comparison of various design choices for **NeuTraL AD** and one of our findings is that its anomaly detection results are robust to the number of learnable transformations.

The same encoder architecture is used for **NeuTraL AD**, **Deep SVDD**, **DROCC**, and with slight modification to achieve the appropriate number of outputs for **DAGMM** and transformation prediction with fixed T. The encoder is a stack of residual blocks of 1d convolutional layers. The number of blocks depends on the dimensionality of the data and is detailed in Appendix B. The encoder has output dimension 64 for all experiments.

Results. The results of **NeuTraL AD** in comparison to the baselines from Section 4.2 on time series datasets from various fields are reported in table 1. **NeuTraL AD** outperforms all shallow baselines in all experiments and outperforms the deep learning baselines in 4 out of 5 experiments. Only on the **RS** data, it is outperformed by transformation prediction with fixed transformations, which we designed to understand the value of learning transformations with **NeuTraL AD** vs using hand-crafted transformations. The results confirm that designing the transformations only succeeds sometimes, whereas with **NeuTraL AD** we can learn the appropriate transformations. The learned transformations also give **NeuTraL AD** a competitive advantage over the other self-supervised baseline **GOAD** which uses random affine transformations. The performance of the shallow anomaly detection baselines hints at the difficulty of each anomaly detection task; the shallow methods perform well on **SAD** and **CT**, but perform worse than the deep learning based methods on other data.

What does NeuTraL AD learn? For visualization purposes, we train **NeuTraL AD** with 4 learnable transformations on the **SAD** data. Figure 3 shows the structure in the

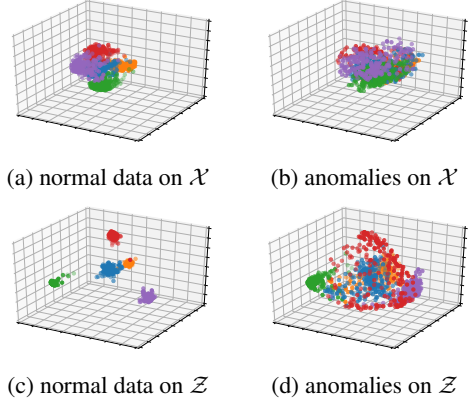


Figure 3. 3D Visualization (projected by PCA) of how the original samples (blue) from the **SAD** dataset and the different views created by the neural transformations of **NeuTraL AD** (one color per transformation type) cluster in data space (Figures 3a and 3b) and in the embedding space of the encoder (Figures 3c and 3d). The crisp separation of the different transformations of held-out inliers (Figure 3c) in contrast to the overlap between transformed anomalies (Figure 3d) visualizes how **NeuTraL AD** is able to detect anomalies.

data space \mathcal{X} and the embedding space of the encoder \mathcal{Z} after training. Held-out data samples (blue) are transformed by each of the learned transformations $T_k(x) = M_k(x) \odot x$ to produce $K = 4$ different views of each sample (the transformations are color coded by the other colors). Projection to three principal components with PCA allows for visualization in 3D. In Figures 3a and 3b we can see that the transformations already cluster together in the data space, but only with the help of the encoder the different views of inliers are separated from each other Figure 3c. In comparison, the anomalies and their transformations are less structured in \mathcal{Z} (Figure 3d), visually explaining why they incur a higher anomaly score and can be detected as anomalies.

The learned masks $M_{1:4}(x)$ of one inlier x are visualized in Figure 4. We can see that the four masks are dissimilar with each other, and have learned to focus on different aspects of the spectrogram. The masks take values between 0 and 1, with dark areas corresponding to values close to 0 that are zeroed out by the masks, while light colors correspond to the areas of the spectrogram that are not masked out. Interestingly, in M_1 , M_2 , and M_3 we can see ‘black lines’ where they mask out entire frequency bands at least for part of the sequence. In contrast, M_4 has a bright spot in the middle left part of the spectrogram; it creates views that focus on the content of the intermediate frequencies at the first half of the recording.

How do the methods cope with an increased variability of inliers? To study this question empirically, we increase

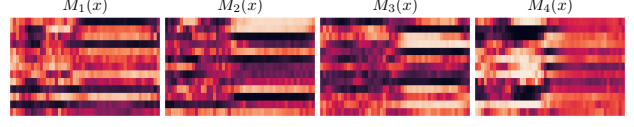


Figure 4. **NeuTraL AD** learns dissimilar masks for **SAD** spectrograms. Dark horizontal lines indicate where M_1 and M_2 mask out frequency bands almost entirely, while the bright spot in the middle left part of M_4 indicates that this mask brings the intermediate frequencies in the first half of the recording into focus.

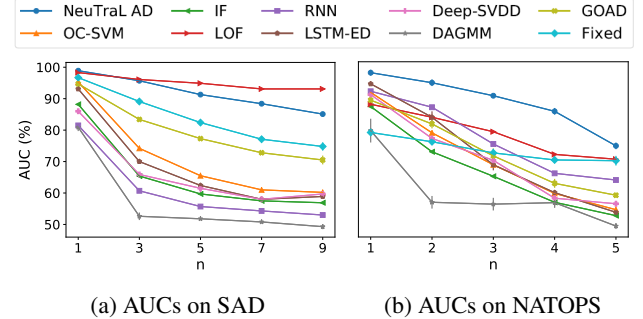


Figure 5. AUC result of n -vs-all experiments on **SAD** and **NATOPS** with error bars (barely visible due to significance).

the number of classes n considered to be inliers. We test all methods on **SAD** and **NATOPS** under the n -vs-rest setting with varying n . Since there are too many combinations of normal classes when n approaches $N - 1$, we only consider combinations of n consecutive classes. From fig. 5 we can observe that the performance of all methods drops as the number of classes included in the normal data increases. This shows that the increased variance in the nominal data makes the task more challenging. **NeuTraL AD** outperforms all baselines on **NATOPS** and all deep-learning baselines on **SAD**. It is interesting that **LOF**, a method based on k -nearest neighbors, performs better than our method (and all other baselines) on **SAD** when n is larger than three.

4.4. Anomaly Detection of Tabular Data

Tabular data is another important application area of anomaly detection. For example, many types of health data come in tabular form. To unleash the power of self-supervised anomaly detection for these domains, [Bergman & Hoshen \(2020\)](#) suggest using random affine transformation. Here we study the benefit of *learning* the transformations with **NeuTraL AD**. We base the empirical study on tabular datasets used in previous work ([Zong et al., 2018](#); [Bergman & Hoshen, 2020](#)) and follow their precedent of reporting results in terms of F1-scores.

Tabular Datasets. We study the four tabular datasets from the empirical studies of [Zong et al. \(2018\)](#); [Bergman & Hoshen \(2020\)](#). The datasets include the small-scale med-

Table 2. F1-score (%) with standard deviation for anomaly detection on tabular datasets (choice of F1-score consistent with prior work).

	Arrhythmia	Thyroid	KDD	KDDRev
OC-SVM	45.8	38.9	79.5	83.2
IF	57.4	46.9	90.7	90.6
LOF	50.0	52.7	83.8	81.6
Deep SVDD	53.9±3.1	70.8±1.8	99.0±0.1	98.6±0.2
DAGMM	49.8	47.8	93.7	93.8
GOAD	52.0±2.3	74.5±1.1	98.4±0.2	98.9±0.3
DROCC	46	27	-	-
NeuTraL AD	60.3±1.1	76.8±1.9	99.3±0.1	99.1±0.1

ical datasets Arrhythmia and Thyroid as well as the large-scale cyber intrusion detection datasets KDD and KDDRev (see appendix C for all relevant details). We follow the configuration of (Zong et al., 2018) to train all models on half of the normal data, and test on the rest of the normal data as well as the anomalies.

Baseline Models. We compare NeuTraL AD to shallow and deep baselines outlined in Section 4.2, namely OC-SVM, IF, LOF, and the deep anomaly detection methods Deep SVDD, DAGMM, GOAD, and DROCC.

Implementation details. The implementation details of OC-SVM, LOF, DAGMM, and GOAD are replicated from Bergman & Hoshen (2020), as we report their results. The implementation of DROCC is from their official code.

The learnable transformations are again parameterized multiplicatively $T_k(x) = M_k(x) \odot x$, with the masks M_k consisting of 3 bias-free linear layers with intermediate ReLU activations and sigmoid activation for the output layer. The number of learnable transformations is 11 for Arrhythmia, 4 for Thyroid, and 7 for KDD and KDDRev.

We use a comparable encoder architecture for NeuTraL AD and Deep SVDD of 3 (4 for KDD and KDDRev) linear layers with ReLU activations. The output dimensions of the encoder are 12 for Thyroid and 32 for the other datasets.

Results. The results of OC-SVM, LOF, DAGMM, and GOAD are taken from (Bergman & Hoshen, 2020). The results of DROCC are provided by Goyal et al. (2020) per email³. NeuTraL AD outperforms all baselines on all datasets. Compared with the self-supervised anomaly detection baseline GOAD, we use much less transformations, and we don't need early stopping in any of the experiments.

4.5. Design Choices for the Transformations

In Section 3.2, we have discussed the advantages of NeuTraL AD for neural transformation learning; no regularization or restrictions on the transformation family are neces-

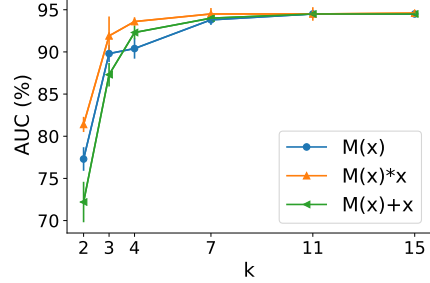


Figure 6. The outlier detection accuracy in terms of AUC of NeuTraL AD on NATOPS increases as the number of transformations K increases, but stabilizes when a certain threshold is reached ($K > \approx 10$). With enough transformations NeuTraL AD is robust to the parametrization of the transformations.

sary to ensure the transformations fulfill the semantics and diversity requirements defined in Section 3.2.

In this Section, we study the performance of NeuTraL AD under various design choices for the learnable transformations, including their parametrization, and their number K . We consider the following parametrizations: *feed forward* $T_k(x) := M_k(x)$, *residual* $T_k(x) := M_k(x) + x$, and *multiplicative* $T_k(x) := M_k(x) \odot x$, which differ in how they combine the learnable masks $M_k(\cdot)$ with the data.

In fig. 6 we show the anomaly detection accuracy achieved with each parametrization, as K varies from 2 to 15 on the time series data NATOPS (and the tabular data Arrhythmia in Appendix D). For large enough K , NeuTraL AD is robust to the different parametrizations, since DCL ensures the learned transformations satisfy the semantic requirement and the diversity requirement. The performance of NeuTraL AD improves as the number k increases, and becomes stable when K is large enough. When $K \leq 4$, the performance has a larger variance, since the learned transformations are not guaranteed to be useful for anomaly detection without the guidance of any labels. When K is large enough, the learned transformations contain with high likelihood some transformations that are useful for anomaly detection.

5. Conclusion

We propose a self-supervised anomaly detection method with learnable transformations. The key ingredient is a novel training objective based on a **deterministic contrastive loss**, which encourages the learned transformations to produce diverse views that each share semantic information with the original sample, while being dissimilar. This unleashes the power of self-supervised anomaly detection to various data types including time series and tabular data. Our extensive empirical study finds, that on these data types, learning transformations and detecting outliers with NeuTraL AD improves over the state of the art.

³results under consistent experimental settings with prior works

Acknowledgements

MK acknowledges support by the Carl-Zeiss Foundation, by the German Research Foundation (DFG) award KL 2698/2-1, and by the Federal Ministry of Science and Education (BMBF) awards 01IS18051A and 031B0770E.

SM was supported by the National Science Foundation (NSF) under Grants 1928718, 2003237 and 2007719, by Qualcomm, and by the Defense Advanced Research Projects Agency (DARPA) under Contract No. HR001120C0021. Any opinions, findings and conclusions or recommendations expressed in this material are those of the author(s) and do not necessarily reflect the views of DARPA.

We acknowledge helpful discussions with Dennis Wagner. We acknowledge Luis Augusto Weber Mercado's contribution to fig. 1. We acknowledge Goyal et al. (2020)'s quick response and updated experiment results.

References

Abati, D., Porrello, A., Calderara, S., and Cucchiara, R. Latent space autoregression for novelty detection. In *Proceedings of the IEEE Conference on Computer Vision and Pattern Recognition*, pp. 481–490, 2019.

Akcay, S., Atapour-Abarghouei, A., and Breckon, T. P. Gandomly: Semi-supervised anomaly detection via adversarial training. In *Asian conference on computer vision*, pp. 622–637. Springer, 2018.

Bachman, P., Hjelm, R. D., and Buchwalter, W. Learning representations by maximizing mutual information across views. *arXiv preprint arXiv:1906.00910*, 2019.

Bagnall, A., Dau, H. A., Lines, J., Flynn, M., Large, J., Bostrom, A., Southam, P., and Keogh, E. The uea multivariate time series classification archive, 2018. *arXiv preprint arXiv:1811.00075*, 2018.

Baragona, R. and Battaglia, F. Outliers detection in multivariate time series by independent component analysis. *Neural computation*, 19(7):1962–1984, 2007.

Bergman, L. and Hoshen, Y. Classification-based anomaly detection for general data. 2020.

Chen, T., Kornblith, S., Norouzi, M., and Hinton, G. A simple framework for contrastive learning of visual representations. In *International conference on machine learning*, pp. 1597–1607. PMLR, 2020.

Chen, X. and Konukoglu, E. Unsupervised detection of lesions in brain mri using constrained adversarial auto-encoders. *arXiv preprint arXiv:1806.04972*, 2018.

Cubuk, E. D., Zoph, B., Mane, D., Vasudevan, V., and Le, Q. V. Autoaugment: Learning augmentation policies from data. *arXiv preprint arXiv:1805.09501*, 2018.

Deecke, L., Vandermeulen, R., Ruff, L., Mandt, S., and Kloft, M. Image anomaly detection with generative adversarial networks. In *Joint european conference on machine learning and knowledge discovery in databases*, pp. 3–17. Springer, 2018.

Doersch, C., Gupta, A., and Efros, A. A. Unsupervised visual representation learning by context prediction. In *Proceedings of the IEEE international conference on computer vision*, pp. 1422–1430, 2015.

Dosovitskiy, A., Fischer, P., Springenberg, J. T., Riedmiller, M., and Brox, T. Discriminative unsupervised feature learning with exemplar convolutional neural networks. *IEEE transactions on pattern analysis and machine intelligence*, 38(9):1734–1747, 2015.

Erfani, S. M., Rajasegarar, S., Karunasekera, S., and Leckie, C. High-dimensional and large-scale anomaly detection using a linear one-class svm with deep learning. *Pattern Recognition*, 58:121–134, 2016.

Gidaris, S., Singh, P., and Komodakis, N. Unsupervised representation learning by predicting image rotations. *arXiv preprint arXiv:1803.07728*, 2018.

Golan, I. and El-Yaniv, R. Deep anomaly detection using geometric transformations. In *Advances in Neural Information Processing Systems*, pp. 9758–9769, 2018.

Goyal, S., Raghunathan, A., Jain, M., Simhadri, H. V., and Jain, P. Drock: Deep robust one-class classification. In *International Conference on Machine Learning*, pp. 3711–3721. PMLR, 2020.

Gutmann, M. and Hyvärinen, A. Noise-contrastive estimation: A new estimation principle for unnormalized statistical models. In *Proceedings of the Thirteenth International Conference on Artificial Intelligence and Statistics*, pp. 297–304. JMLR Workshop and Conference Proceedings, 2010.

Gutmann, M. U. and Hyvärinen, A. Noise-contrastive estimation of unnormalized statistical models, with applications to natural image statistics. *Journal of Machine Learning Research*, 13(2), 2012.

Hadsell, R., Chopra, S., and LeCun, Y. Dimensionality reduction by learning an invariant mapping. In *2006 IEEE Computer Society Conference on Computer Vision and Pattern Recognition (CVPR'06)*, volume 2, pp. 1735–1742. IEEE, 2006.

Hendrycks, D., Mazeika, M., and Dietterich, T. Deep anomaly detection with outlier exposure. *arXiv preprint arXiv:1812.04606*, 2018.

Hendrycks, D., Mazeika, M., Kadavath, S., and Song, D. Using self-supervised learning can improve model robustness and uncertainty. In *Advances in Neural Information Processing Systems*, pp. 15663–15674, 2019.

Hjelm, R. D., Fedorov, A., Lavoie-Marchildon, S., Grewal, K., Bachman, P., Trischler, A., and Bengio, Y. Learning deep representations by mutual information estimation and maximization. *arXiv preprint arXiv:1808.06670*, 2018.

Ho, D., Liang, E., Chen, X., Stoica, I., and Abbeel, P. Population based augmentation: Efficient learning of augmentation policy schedules. In *International Conference on Machine Learning*, pp. 2731–2741. PMLR, 2019.

Hyndman, R. J., Wang, E., and Laptev, N. Large-scale unusual time series detection. In *2015 IEEE international conference on data mining workshop (ICDMW)*, pp. 1616–1619. IEEE, 2015.

Kieu, T., Yang, B., and Jensen, C. S. Outlier detection for multidimensional time series using deep neural networks. In *2018 19th IEEE International Conference on Mobile Data Management (MDM)*, pp. 125–134. IEEE, 2018.

Kim, K. H., Shim, S., Lim, Y., Jeon, J., Choi, J., Kim, B., and Yoon, A. S. Rapp: Novelty detection with reconstruction along projection pathway. In *International Conference on Learning Representations*, 2019.

Lim, S., Kim, I., Kim, T., Kim, C., and Kim, S. Fast autoaugment. *arXiv preprint arXiv:1905.00397*, 2019.

Linsker, R. Self-organization in a perceptual network. *Computer*, 21(3):105–117, 1988.

Liu, F. T., Ting, K. M., and Zhou, Z.-H. Isolation forest. In *2008 Eighth IEEE International Conference on Data Mining*, pp. 413–422. IEEE, 2008.

Malhotra, P., Ramakrishnan, A., Anand, G., Vig, L., Agarwal, P., and Shroff, G. Lstm-based encoder-decoder for multi-sensor anomaly detection. *arXiv preprint arXiv:1607.00148*, 2016.

Misra, I., Zitnick, C. L., and Hebert, M. Shuffle and learn: unsupervised learning using temporal order verification. In *European Conference on Computer Vision*, pp. 527–544. Springer, 2016.

Mnih, A. and Kavukcuoglu, K. Learning word embeddings efficiently with noise-contrastive estimation. *Advances in neural information processing systems*, 26:2265–2273, 2013.

Munir, M., Siddiqui, S. A., Dengel, A., and Ahmed, S. Deepant: A deep learning approach for unsupervised anomaly detection in time series. *IEEE Access*, 7:1991–2005, 2018.

Noroozi, M. and Favaro, P. Unsupervised learning of visual representations by solving jigsaw puzzles. In *European conference on computer vision*, pp. 69–84. Springer, 2016.

Oord, A. v. d., Li, Y., and Vinyals, O. Representation learning with contrastive predictive coding. *arXiv preprint arXiv:1807.03748*, 2018.

Perera, P., Nallapati, R., and Xiang, B. Ogan: One-class novelty detection using gans with constrained latent representations. In *Proceedings of the IEEE Conference on Computer Vision and Pattern Recognition*, pp. 2898–2906, 2019.

Principi, E., Vesperini, F., Squartini, S., and Piazza, F. Acoustic novelty detection with adversarial autoencoders. In *2017 International Joint Conference on Neural Networks (IJCNN)*, pp. 3324–3330. IEEE, 2017.

Ratner, A. J., Ehrenberg, H. R., Hussain, Z., Dunnmon, J., and Ré, C. Learning to compose domain-specific transformations for data augmentation. *Advances in neural information processing systems*, 30:3239, 2017.

Ruff, L., Vandermeulen, R., Goernitz, N., Deecke, L., Siddiqui, S. A., Binder, A., Müller, E., and Kloft, M. Deep one-class classification. In *International conference on machine learning*, pp. 4393–4402, 2018.

Ruff, L., Vandermeulen, R. A., Görnitz, N., Binder, A., Müller, E., Müller, K.-R., and Kloft, M. Deep semi-supervised anomaly detection. *arXiv preprint arXiv:1906.02694*, 2019a.

Ruff, L., Zemlyanskiy, Y., Vandermeulen, R., Schnake, T., and Kloft, M. Self-attentive, multi-context one-class classification for unsupervised anomaly detection on text. In *Proceedings of the 57th Annual Meeting of the Association for Computational Linguistics*, pp. 4061–4071, 2019b.

Ruff, L., Kauffmann, J. R., Vandermeulen, R. A., Montavon, G., Samek, W., Kloft, M., Dietterich, T. G., and Müller, K.-R. A unifying review of deep and shallow anomaly detection. *arXiv preprint arXiv:2009.11732*, 2020.

Ruiz, A. P., Flynn, M., Large, J., Middlehurst, M., and Bagall, A. The great multivariate time series classification bake off: a review and experimental evaluation of recent algorithmic advances. *Data Mining and Knowledge Discovery*, pp. 1–49, 2020.

Schlegl, T., Seeböck, P., Waldstein, S. M., Schmidt-Erfurth, U., and Langs, G. Unsupervised anomaly detection with generative adversarial networks to guide marker discovery. In *International conference on information processing in medical imaging*, pp. 146–157. Springer, 2017.

Shen, L., Li, Z., and Kwok, J. Timeseries anomaly detection using temporal hierarchical one-class network. In *Advances in Neural Information Processing Systems*, 2020.

Sohn, K., Li, C.-L., Yoon, J., Jin, M., and Pfister, T. Learning and evaluating representations for deep one-class classification. *arXiv preprint arXiv:2011.02578*, 2020.

Tack, J., Mo, S., Jeong, J., and Shin, J. Csi: Novelty detection via contrastive learning on distributionally shifted instances. *arXiv preprint arXiv:2007.08176*, 2020.

Tamkin, A., Wu, M., and Goodman, N. Viewmaker networks: Learning views for unsupervised representation learning. *arXiv preprint arXiv:2010.07432*, 2020.

Tran, T., Pham, T., Carneiro, G., Palmer, L., and Reid, I. A bayesian data augmentation approach for learning deep models. *arXiv preprint arXiv:1710.10564*, 2017.

Tschannen, M., Djolonga, J., Rubenstein, P. K., Gelly, S., and Lucic, M. On mutual information maximization for representation learning. *arXiv preprint arXiv:1907.13625*, 2019.

Wang, J., Sun, S., and Yu, Y. Multivariate triangular quantile maps for novelty detection. In *Advances in Neural Information Processing Systems*, pp. 5060–5071, 2019a.

Wang, S., Zeng, Y., Liu, X., Zhu, E., Yin, J., Xu, C., and Kloft, M. Effective end-to-end unsupervised outlier detection via inlier priority of discriminative network. In *Advances in Neural Information Processing Systems*, pp. 5962–5975, 2019b.

Wong, E. and Kolter, J. Z. Learning perturbation sets for robust machine learning. *arXiv preprint arXiv:2007.08450*, 2020.

Zhang, R., Isola, P., and Efros, A. A. Split-brain autoencoders: Unsupervised learning by cross-channel prediction. In *Proceedings of the IEEE Conference on Computer Vision and Pattern Recognition*, pp. 1058–1067, 2017.

Zhang, X., Wang, Q., Zhang, J., and Zhong, Z. Adversarial autoaugment. *arXiv preprint arXiv:1912.11188*, 2019.

Zhou, C. and Paffenroth, R. C. Anomaly detection with robust deep autoencoders. In *Proceedings of the 23rd ACM SIGKDD International Conference on Knowledge Discovery and Data Mining*, pp. 665–674, 2017.

Zong, B., Song, Q., Min, M. R., Cheng, W., Lumezanu, C., Cho, D., and Chen, H. Deep autoencoding gaussian mixture model for unsupervised anomaly detection. In *International Conference on Learning Representations*, 2018.

A. Proofs for Section 3.2

In this Appendix, we prove the propositions in Section 3.2. The point is to compare various potential loss functions for neural transformation learning in their ability to produce useful transformations for self-supervised anomaly detection.

Requirements 1 and 2 formalize what we consider useful transformations. The learned transformations should produce diverse views that share semantic information with the original sample.

We give two example edge-cases that violate the requirements, the ‘constant’ edge-case in which the transformed views do no longer depend on the original sample (this violates the semantic requirement) and the ‘identity’ edge-case in which all transformations reproduce the original sample perfectly but violate the diversity requirement.

We compare what happens to various losses for self-supervised anomaly detection under these edge cases. Specifically, we compare the loss of our method \mathcal{L} (Equation (2)) to the transformation prediction loss \mathcal{L}_P (Equation (4)) of Wang et al. (2019b), and the SimCLR loss \mathcal{L}_C (Equation (5), Chen et al. (2020)), which has been used for anomaly detection in Sohn et al. (2020) and Tack et al. (2020). In the original sources these losses have been used with fixed transformations (typically image transformations like rotations, cropping, blurring, etc.). Here we consider the same losses but with the learnable transformations parameterized as defined in Section 3.1. All notation has been defined in Section 3.1.

A.1. Proof of Proposition 1

We first investigate whether we can optimize the transformation prediction loss Equation (4) with respect to the transformation parameters θ_k and the parameters of f_ϕ and obtain learned transformations that fulfil Requirements 1 and 2.

The proposition below states that a constant edge-case can achieve a global minimum of Equation (4), this means that minimizing it can produce transformations that violate Requirement 1.

Proposition 1. *The ‘constant’ edge-case $f_\phi(T_k(x)) = Cc_k$, where c_k is a one-hot vector encoding the k^{th} position (i.e. $c_{kk} = 1$) tends towards the minimum of \mathcal{L}_P (Equation (4)) as the constant C goes to infinity.*

Proof. As a negative log probability $\mathcal{L}_P \geq 0$ is lower bounded by 0. We want to show that with $f_\phi(T_k(x)) = Cc_k$, (where c_k is a one hot vector and C is a constant,) \mathcal{L} goes to 0 as C goes to infinity. Plugging $f_\phi(T_k(x)) = Cc_k$ into \mathcal{L}_P and taking the limit yields

$$\begin{aligned} \lim_{C \rightarrow \infty} \mathcal{L}_P &= \lim_{C \rightarrow \infty} \mathbb{E}_{x \sim \mathcal{D}} \left[- \sum_{k=1}^K \log \frac{\exp C}{\exp C + K - 1} \right] = \lim_{C \rightarrow \infty} -K \log \frac{\exp C}{\exp C + K - 1} \\ &= \lim_{C \rightarrow \infty} -KC + K \log(\exp C + K - 1) = 0 \end{aligned}$$

□

A.2. Proof of Proposition 2

Next, we ask what would happen if we optimized the SimCLR loss \mathcal{L}_C (Equation (5)) with respect to the transformation parameters and the encoder.

The result is, that if we allowed the encoder f_ϕ to be as flexible as necessary to achieve a global minimum of \mathcal{L}_C , then we can derive another minimum of \mathcal{L}_C that relies only on identity transformations, thereby obtaining a solution to the minimization problem that violates the diversity requirement.

Proposition 2. *The ‘identity’ edge-case $T_k(x) = x$ with adequate encoder f_ϕ is a minimizer of \mathcal{L}_C (Equation (5)).*

Proof. $\mathcal{L}_c(\mathcal{M})$ can be separated as the alignment term and the uniformity term.

$$\begin{aligned} \mathcal{L}_c(\mathcal{M}) &= \underbrace{\sum_{i=1}^N \left[-\log h(x_1^{(i)}, x_2^{(i)}) - \log h(x_2^{(i)}, x_1^{(i)}) \right]}_{\mathcal{L}_{\text{alignment}}} \\ &\quad + \underbrace{\sum_{i=1}^N \left[\log \left[\sum_{j=1}^N h(x_1^{(i)}, x_2^{(j)}) + \sum_{j=1}^N \mathbb{1}_{[j \neq i]} h(x_1^{(i)}, x_1^{(j)}) \right] + \log \left[\sum_{j=1}^N h(x_2^{(i)}, x_1^{(j)}) + \sum_{j=1}^N \mathbb{1}_{[j \neq i]} h(x_2^{(i)}, x_2^{(j)}) \right] \right]}_{\mathcal{L}_{\text{uniformity}}}. \end{aligned} \quad (6)$$

A sufficient condition of $\min(\mathcal{L}_c(\mathcal{M}))$ is both $\mathcal{L}_{\text{alignment}}$ and $\mathcal{L}_{\text{uniformity}}$ are minimized.

$$\min(\mathcal{L}_c(\mathcal{M})) \geq \min(\mathcal{L}_{\text{alignment}}) + \min(\mathcal{L}_{\text{uniformity}}). \quad (7)$$

Given an adequate encoder f_ϕ^* , that is flexible enough to minimize both $\mathcal{L}_{\text{alignment}}$ and $\mathcal{L}_{\text{uniformity}}$ for all transformation pairs T_1 and T_2 , we will show we can construct another solution to the minimization problem that relies only on identity transformations.

The alignment term is only minimized for all T_1, T_2 , if $f_\phi^*(T_1(x^{(i)})) = f_\phi^*(T_2(x^{(i)}))$ for all $x^{(i)} \sim \mathcal{M}$. So we know for f_ϕ^* that

$$f_\phi^* = \arg \min_{f_\phi} \mathcal{L}_{\text{alignment}} \iff \text{sim}(f_\phi^*(T_1(x^{(i)})), f_\phi^*(T_2(x^{(i)}))) = 1 \quad \forall x^{(i)} \sim \mathcal{M} \quad (8)$$

$$\iff f_\phi^*(T_1(x^{(i)})) = f_\phi^*(T_2(x^{(i)})) \quad \forall x^{(i)} \sim \mathcal{M}. \quad (9)$$

Define $\tilde{f}_\phi = f_\phi^* \circ T_1$. Since $f_\phi^*(T_1(x^{(i)})) = f_\phi^*(T_2(x^{(i)}))$,

$$\tilde{f}_\phi(\mathbb{I}(x^{(i)})) = f_\phi^*(T_1(x^{(i)})) = f_\phi^*(T_2(x^{(i)})) \quad \forall x^{(i)} \sim \mathcal{M}. \quad (10)$$

Using only the identity transformation $\mathbb{I}(x) = x$ for T_1 and T_2 , and \tilde{f}_ϕ as the encoder in \mathcal{L}_C yields the same minimal loss as under T_1, T_2 and f_ϕ^* . \square

A.3. Proof of Proposition 3

Finally, we investigate the effect of the edge-cases from Propositions 1 and 2 on our objective Equation (2).

Proposition 3. *The edge-cases of Propositions 1 and 2 do not minimize \mathcal{L} (DCL, Equation (2)).*

We divide the proposition and its proof into two parts.

Proposition 3, Part 1. *The ‘constant’ edge-case $f_\phi(T_k(x)) = C c_k$, where c_k is a one-hot vector encoding the k^{th} position (i.e. $c_{kk} = 1$) does not minimize \mathcal{L} (DCL, Equation (2)) for any C , also not as C tends to infinity.*

Proof. We prove $\nabla_\theta \mathcal{L}(x) \neq 0$ in the ‘constant’ edge-case. For simplicity, we define $z_k := f_\phi(T_k(x))$, and $z := f_\phi(x)$. The gradient of $\mathcal{L}(x)$ with respect to the parameters is

$$\begin{aligned} \nabla_\theta \mathcal{L}(x) &= \sum_{k=1}^K \left[-\nabla_\theta \text{sim}(z_k, z) + \frac{h(x_k, x) \nabla_\theta \text{sim}(z_k, z) + \sum_{l \neq k} h(x_k, x_l) \nabla_\theta \text{sim}(z_k, z_l)}{h(x_k, x) + \sum_{l \neq k} h(x_k, x_l)} \right] \\ &= \sum_{k=1}^K \left[\frac{(h(x_k, x) - h(x_k, x) - \sum_{l \neq k} h(x_k, x_l)) \nabla_\theta \text{sim}(z_k, z) + \sum_{l \neq k} h(x_k, x_l) \nabla_\theta \text{sim}(z_k, z_l)}{h(x_k, x) + \sum_{l \neq k} h(x_k, x_l)} \right] \\ &= \sum_{k=1}^K \left[\frac{\sum_{l \neq k} h(x_k, x_l) (\nabla_\theta \text{sim}(z_k, z_l) - \nabla_\theta \text{sim}(z_k, z))}{h(x_k, x) + \sum_{l \neq k} h(x_k, x_l)} \right], \end{aligned} \quad (11)$$

where the score function $h(\cdot)$ (Equation (1)) is larger than zero. We plug $z_k := f_\phi(T_k(x)) = Cc_k$ into Equation (11).

$$\nabla_\theta \mathcal{L}(x) = \sum_{k=1}^K \left[\frac{\sum_{l \neq k} (\nabla_\theta \text{sim}(Cc_k, Cc_l) - \nabla_\theta \text{sim}(Cc_k, z))}{h(Cc_k, x) + K - 1} \right] \quad (12)$$

$$\nabla_\theta \mathcal{L}(x) = \sum_{k=1}^K \left[\frac{\sum_{l \neq k} (\nabla_\theta \text{sim}(c_k, c_l) - \nabla_\theta \text{sim}(c_k, z))}{h(c_k, x) + K - 1} \right], \quad (13)$$

where the second line is obtained by using the fact that the cosine similarity only depends on the normalized vectors and hence C can be dropped.

As $c_k \perp c_l$, $\nabla_\theta \text{sim}(c_k, c_l) - \nabla_\theta \text{sim}(c_k, z) \leq 0$, and the equality is true only if $c_l = z/|z|$. So, the sufficient and necessary condition of $\nabla_\theta \mathcal{L}(x) = 0$ is $\forall k, c_k = z/|z|$. As $c_k \neq c_l$, it contradicts with the sufficient and necessary condition. Therefore, $\nabla_\theta \mathcal{L}(x) \neq 0$ and the ‘constant’ edge-case cannot be a minimizer of \mathcal{L} . \square

Proposition 3, Part 2. *The ‘identity’ edge-case $T_k(x) = x$ does not minimize \mathcal{L} (Equation (2)) for adequate encoder f_ϕ .*

Proof. Plugging $T_k(x) = x$ for all k into Equation (2)

$$\mathcal{L} = \mathbb{E}_{x \sim \mathcal{D}} \left[- \sum_{k=1}^K \log \frac{h(x, x)}{Kh(x, x)} \right] = K \log K. \quad (14)$$

This is K times the cross-entropy of the uniform distribution, meaning that using the identity transformation is equivalent to random guessing for the task of the **DCL**, which is to predict which sample is the original given a transformed view. When f_ϕ is adequate (i.e. flexible enough) we can do better than random on \mathcal{L} . This can be seen in the anomaly scores in Figure 2b which are well above $-K \log K$ after training (better than random).

We can also construct examples which achieve better than random performance. For example, for $K = 2$, taking $z_1 \perp z$, $z_2 \perp z$, and $z_1 = -z_2$, does better than random. The loss values (with $\tau = 1$) of the two cases are

- ‘Identity’ edge-case: $z_1 = z_2 = z$, so $\mathcal{L}(x) = -2 \log(0.5) = 1.386$.
- Counter example: $z_1 \perp z$, $z_2 \perp z$, and $z_1 = -z_2$, so $\mathcal{L}(x) = -2 \log(1/(1 + \exp(-1))) = 0.627$.

The counter example achieves a lower loss value than the ‘identity’ edge-case. So the ‘identity’ edge-case is not the minimum of $\mathcal{L}(x)$. \square

B. Implementation details

B.1. Implementations of NeuTraL AD in time series datasets

The encoder used in all experiments consists of residual blocks of 1d convolutional layers with kernel size of 3, padding of 1, and stride of 1 or 2 for downsampling, as well as one 1d convolutional layer on the top of all residual blocks, which is used to reduce the dimensions to the latent dimension 64. The detailed network structure (from bottom to top) in each time series dataset is:

- **SAD**: (i) one residual block with the stride of 1, and the output dimension of 32. (ii) four residual blocks with the stride of 2, and the output dimensions of 32, 64, 128, 256. (iii) one 1d convolutional layer of kernel size of 6.
- **NATOPS**: (i) one residual block with the stride of 1, and the output dimension of 32. (ii) four residual blocks with the stride of 2, and the output dimensions of 32, 64, 128, 256. (iii) one 1d convolutional layer of kernel size of 4.
- **CT**: (i) one residual block with the stride of 1, and the output dimension of 32. (ii) six residual blocks with the stride of 2, and the output dimensions of 32, 64, 128, 256, 256, 256. (iii) one 1d convolutional layer of kernel size of 3.
- **EPSY**: (i) one residual block with the stride of 1, and the output dimension of 32. (ii) six residual blocks with the stride of 2, and the output dimensions of 32, 64, 128, 256, 256, 256. (iii) one 1d convolutional layer of kernel size of 4.
- **RS**: (i) one residual block with the stride of 1, and the output dimension of 32. (ii) three residual blocks with the stride of 2, and the output dimensions of 32, 64, 128. (iii) one 1d convolutional layer of kernel size of 4.

B.2. Implementations of baselines

- Traditional Anomaly Detection Baselines. **OC-SVM**, **IF**, and **LOF** are taken from scikit-learn library with default parameters.
- Deep Anomaly Detection Baselines. The implementations of **Deep SVDD**, **DROCC**, and **DAGMM** are adopted from the published codes with a similar encoder as **NeuTraL AD**. **DAGMM** has a hyperparameter of the number of mixture components. We consider the number of components between 4 and 12 and select the best performing one.
- Self-supervised Anomaly Detection Baselines. The implementation of **GOAD** is taken from the published code. The results of **GOAD** depend on the choice of the output dimension r of affine transformations. We consider the reduced dimension $r \in \{2^2, 2^3, \dots, 2^6\}$, and select the best performing one. We craft specific time-series transformations for the designed classification-based baseline. The hand-crafted transformations are the compositions of flipping along time axis (true/false), flipping along channel axis (true/false), and shifting along time axis by 0.25 of its time length (forward/backward/none). By taking all possible compositions, we obtain a total of $2 * 2 * 3 = 12$ transformations.
- Anomaly Detection Baselines for Time Series. The **RNN** is parameterized by a two layers recurrent neural networks, e.g. GRU, and a stack of two linear layers with ReLU activation on the top of it which outputs the mean and variance at each time step. The implementation of **LSTM-ED** is taken from the web.

C. Tabular datasets

The four used tabular datasets are:

- Arrhythmia: A cardiology dataset from the UCI repository contains 274 continuous attributes and 5 categorical attributes. Following the data preparation of previous works, only 274 continuous attributes are considered. The abnormal classes include 3, 4, 5, 7, 8, 9, 14, and 15. The rest classes are considered as normal.
- Thyroid: A medical dataset from the UCI repository contains attributes related to hyperthyroid diagnosis. Following the data preparation of previous works, only 6 continuous attributes are considered. The hyperfunction class is treated as abnormal, and the rest 2 classes are considered as normal.
- KDDCUP: The KDDCUP99 10 percent dataset from the UCI repository contains 34 continuous attributes and 7 categorical attributes. Following the data preparation of previous works, 7 categorical attributes are represented by one-hot vectors. Eventually, the data has 120 dimensions. The attack samples are considered as normal, and the non-attack samples are considered as abnormal.
- KDDCUP-Rev: It is derived from the KDDCUP99 10 percent dataset. The non-attack samples are considered as normal, and attack samples are considered as abnormal. Following the data preparation of previous works, attack data is sub-sampled to consist of 25% of the number of non-attack samples.

D. Additional quantitative results on time series datasets

We study the performance of all models on all used time series datasets under the n -vs-rest setting, where $n = N - 1$. Thus, only one class is considered as anomalies, and the rest $N - 1$ classes are normal. The results are reported in table 3. We can see, the performance of all deep learning based methods drops because of the increased variability of normal data. Our method outperforms other deep learning methods on 4 of 5 datasets. On the **RS**, it is outperformed by transformation prediction with hand-crafted transformations. The results are consistent with the experiments under one-vs.-rest setting. The traditional method **LOF** performs better than deep learning methods also on **CT** besides **SAD**.

In fig. 7 we show the F1-score achieved with each parametrization (*feed forward* $T_k(x) := M_k(x)$, *residual* $T_k(x) := M_k(x) + x$, and *multiplicative* $T_k(x) := M_k(x) \odot x$), as K varies from 2 to 15 on the tabular data Arrhythmia. The performance of **NeuTraL AD** improves as the number K increases, and becomes stable when K is large enough. For large enough K , **NeuTraL AD** is robust to the different parametrizations.

Table 3. Average AUC with standard deviation for n -vs-rest ($n = N - 1$) anomaly detection on time series datasets.

	SAD	NATOPS	CT	EPSY	RS
OC-SVM	60.2	57.6	57.8	50.2	55.9
IF	56.9	56.0	57.9	55.3	58.4
LOF	93.1	71.2	90.3	54.7	59.4
RNN	53.0 ± 0.1	65.6 ± 0.4	55.7 ± 0.8	74.9 ± 1.5	75.8 ± 0.9
LSTM-ED	58.9 ± 0.5	56.9 ± 0.7	50.9 ± 1.2	56.8 ± 2.1	63.1 ± 0.6
Deep SVDD	59.7 ± 0.5	59.2 ± 0.8	54.4 ± 0.7	52.9 ± 1.4	62.2 ± 2.1
DAGMM	49.3 ± 0.8	53.2 ± 0.8	47.5 ± 2.5	52.0 ± 1.0	47.8 ± 3.5
GOAD	70.5 ± 1.4	61.5 ± 0.7	81.1 ± 0.1	62.7 ± 0.9	68.2 ± 0.9
fixed Ts	74.8 ± 1.3	70.8 ± 1.3	63.0 ± 0.6	69.8 ± 1.6	81.6 ± 1.2
NeuTraL AD	85.1 ± 0.3	74.8 ± 0.9	87.4 ± 0.2	80.5 ± 1.0	80.0 ± 0.4

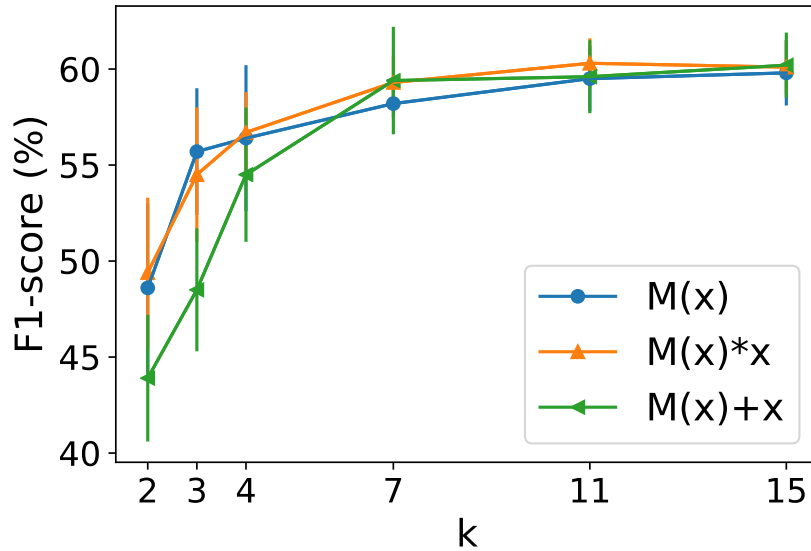


Figure 7. The outlier detection accuracy in terms of F1-score of NeuTraL AD on arrhythmia increases as the number of transformations K increases, but stabilizes when a certain threshold is reached ($K > \approx 10$). With enough transformations NeuTraL AD is robust to the parametrization of the transformations.

E. Additional qualitative results

E.1. Results for time series data

In fig. 8, we show the learned transformations (parameterized as $T(x) = M(x) \odot x$ and $K = 4$) on spoken Arabic digits. The learned transformations given one normal example are shown on the first row. The learned transformations given one example of each abnormal class are shown on the following rows.

In fig. 9, we show the learned transformations (parameterized as $T(x) = M(x)$ and $K = 4$) on NATOPS. The learned transformations given one normal example are shown on the first row. The learned transformations given one example of each abnormal class are shown on the following rows.

E.2. Results for tabular data

The learned transformations of thyroid, which are visualized in fig. 10, offer us the possible explanations of why a data instance is an anomalies. We illustrate one normal example, and three anomalies on the first row. Since the anomaly score eq. (3) is the sum of terms caused by each transformation. Each score shown on the last row has four bars indicating the terms caused by each transformation. The score of the normal example is very low, and its bars are invisible from the plot. The scores of three anomalies are mainly contributed by different terms (colored with orange). The four learned masks are colored with blue and listed on four rows. M_4 focuses on checking the value of the fourth attribute, and contributes high

values to the scores of all listed anomalies. In comparison, M_2 is less useful for anomaly detection. **NeuTraL AD** is able to learn diverse transformations, but is not guaranteed to learn transformations that are useful for anomaly detection, since no label is included in the training.

We project the score terms of test data contributed by T_1 , T_3 , and T_4 to a simplex to visualize which transformation dominates the anomaly score in fig. 11. From the left subplot, we can see, the scores of normal data (blue) are not dominated by any single transformation, while the scores of anomalies are mainly dominated by T_3 and T_4 . In the right subplot, we visualize the magnitudes of scores via the transparency. We can see, the score magnitudes of normal data are clearly lower than the score magnitudes of anomalies.

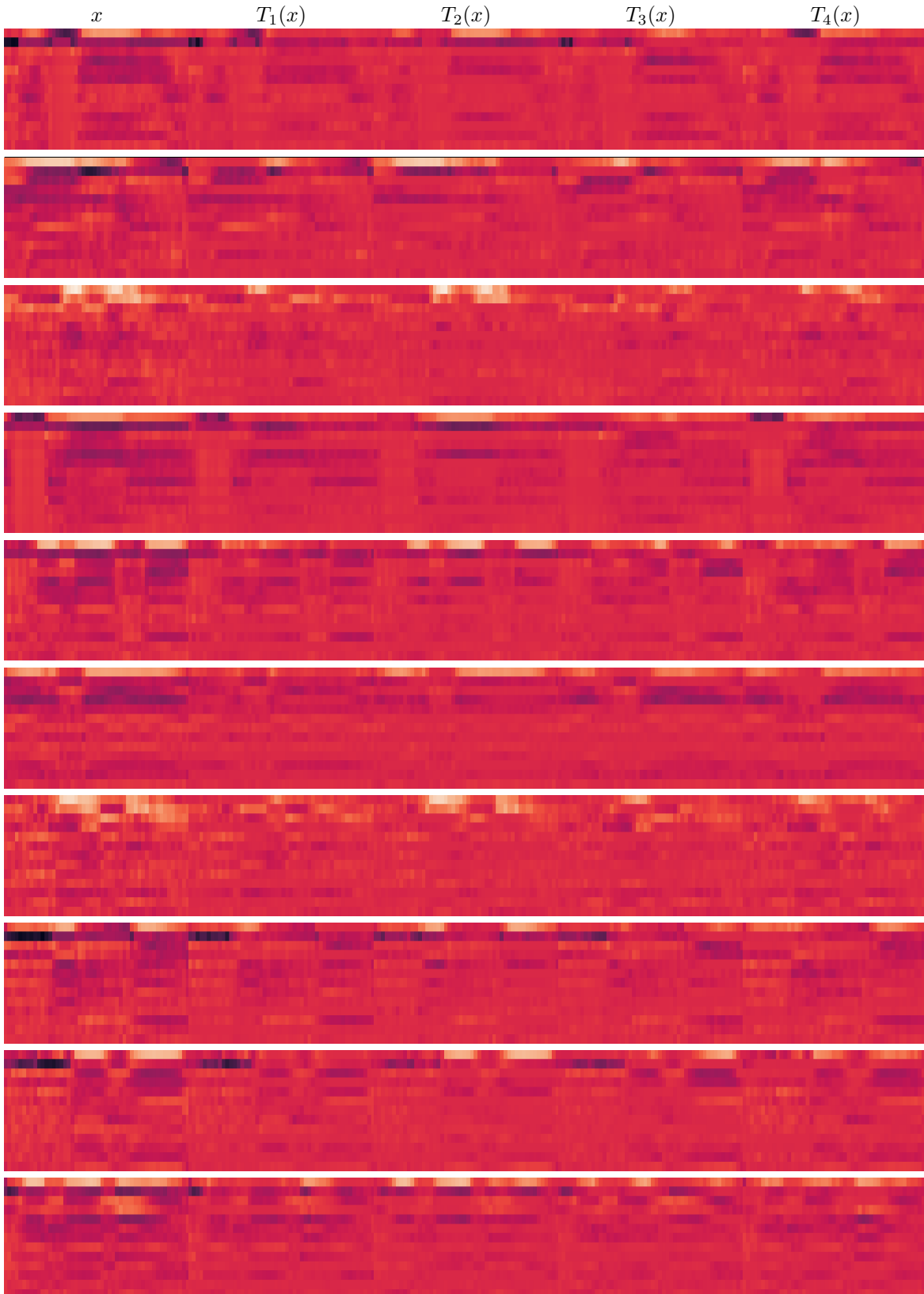


Figure 8. The learned transformations ($T(x) = M(x) \odot x$) on SAD. The first row: the learned transformations given one example of the normal class. The rest rows: the learned transformations given one example of each abnormal class.

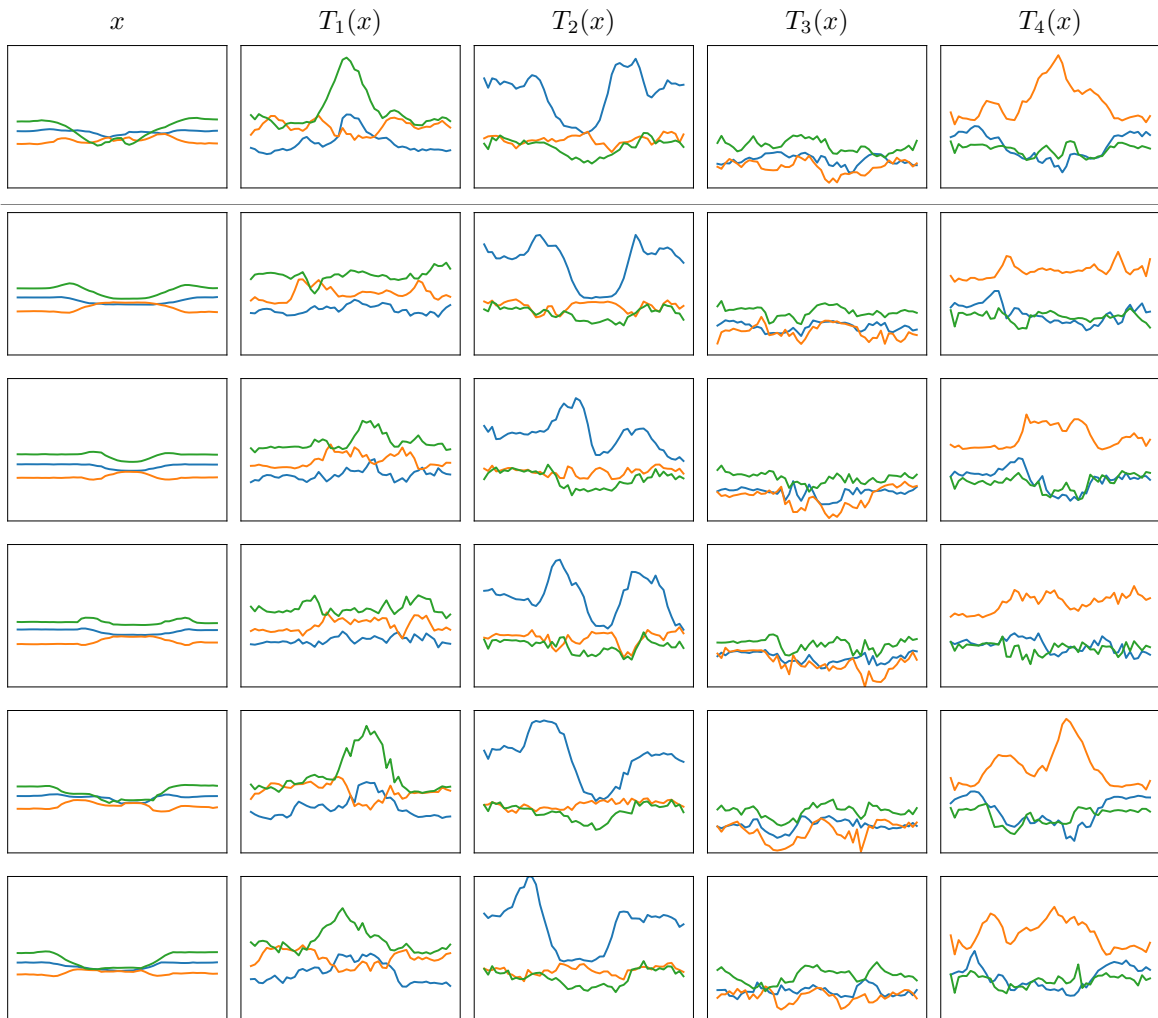


Figure 9. The learned transformations ($T(x) = M(x)$) on NATOPS. The first row: the learned transformations given one example of the normal class. The rest rows: the learned transformations given one example of each abnormal class.



Figure 10. Visualizations of thyroid. The first row: one normal example and three abnormal examples. The second to the fourth rows: the learned four masks of them. The fifth row: the scores contributed by each transformation of them, where the highest term is colored by orange. The plots on each row are under the same scale.

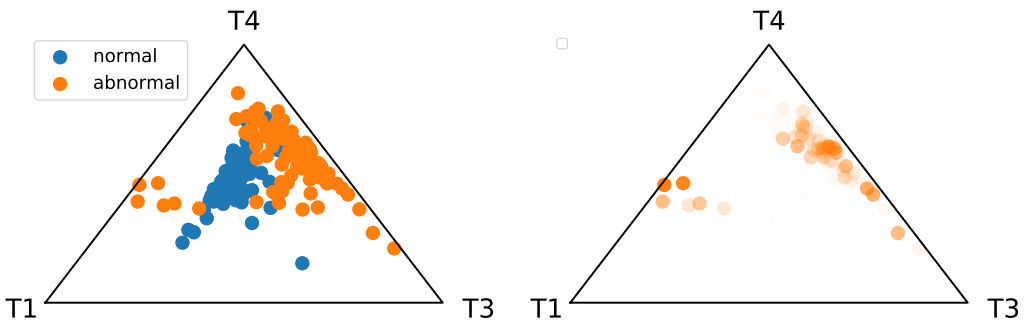


Figure 11. Visualizations of thyroid. We project the scores contributed by T_1 , T_3 , and T_4 to a simplex. The subplot on the left visualizes which transformation dominates the score. The subplot on the right visualizes the scores via the transparency.